

## Differences in Virus-Induced Cell Morphology and in Virus Maturation between MVA and Other Strains (WR, Ankara, and NYCBH) of Vaccinia Virus in Infected Human Cells

Juan Carlos Gallego-Gómez,<sup>1,2</sup> Cristina Risco,<sup>2</sup> Dolores Rodríguez,<sup>1</sup> Pilar Cabezas,<sup>2</sup>  
Susana Guerra,<sup>1</sup> José L. Carrascosa,<sup>2</sup> and Mariano Esteban<sup>1\*</sup>

*Department of Molecular and Cellular Biology<sup>1</sup> and Department of Structure of Macromolecules,<sup>2</sup>  
Centro Nacional de Biotecnología, Consejo Superior de Investigaciones Científicas,  
Campus Universidad Autónoma, 28049 Madrid, Spain*

Received 19 February 2003/Accepted 2 July 2003

**Live recombinants based on attenuated modified vaccinia virus Ankara (MVA) are potential vaccine candidates against a broad spectrum of diseases and tumors. To better understand the efficacy of MVA as a human vaccine, we analyzed by confocal and electron microscopy approaches MVA-induced morphological changes and morphogenetic stages during infection of human HeLa cells in comparison to other strains of vaccinia virus (VV): the wild-type Western Reserve (WR), Ankara, and the New York City Board of Health (NYCBH) strains. Confocal microscopy studies revealed that MVA infection alters the cytoskeleton producing elongated cells (bipolar), which do not form the characteristic actin tails. Few virions are detected in the projections connecting neighboring cells. In contrast, cells infected with the WR, Ankara, and NYCBH strains exhibit a stellated (multipolar) or rounded morphology with actin tails. A detailed transmission electron microscopy analysis of HeLa cells infected with MVA showed important differences in fine ultrastructure and amounts of the viral intermediates compared to cells infected with the other VV strains. In HeLa cells infected with MVA, the most abundant viral forms are intracellular immature virus, with few intermediates reaching the intracellular mature virus (IMV) form, at various stages of maturation, which exhibit a more rounded shape than IMVs from cells infected with the other VV strains. The “IMVs” from MVA-infected cells have an abnormal internal structure (“atypical” viruses) with potential alterations in the core-envelope interactions and are unable to significantly acquire the additional double envelope to render intracellular envelope virus. The presence of potential cell-associated envelope virus is very scarce. Our findings revealed that MVA in human cells promotes characteristic morphological changes to the cells and is able to reach the IMV stage, but these virions were not structurally normal and the subsequent steps in the morphogenetic pathway are blocked.**

The use of viral vectors as tools for basic research and vaccination models has been developed considerably during the last two decades (2, 6, 16). In this sense, vaccinia virus (VV) has been widely used because of its ability to carry large inserts of foreign genes (11, 35). VV, the prototype member of the *Poxviridae* family, is a large DNA virus whose replication and assembly occurs entirely in the cytoplasm of the host cell (31). VV is an ideal model for the expression of foreign antigens because they are expressed to produce recombinant proteins that will undergo the same posttranslational modifications as when expressed in the natural context (5, 23, 24). Moreover, the early genes of VV cause a shutoff of the host cell protein synthesis, whereas the expression of foreign proteins is favored (6, 31). This virus-cell system is an excellent model for molecular and cellular biologists to understand fundamental questions in cell biology and also for immunologists in the study of immune responses (11, 34, 42, 48, 50, 52).

A main goal of vaccination programs is the development of safe and efficient vectors. Due to its characteristics as potential vaccine, the attenuated modified VV Ankara (MVA) has been

studied during the past few years (2, 3, 8, 33, 36, 53). The wild-type strains of VV are cytopathogenic and virulent in mice, producing new rounds of virus replication, which is a drawback for repeated immunization purposes. In contrast, MVA has been included in a number of trials, in which it has been shown to be a safe vector and to induce immune protective responses in animal model systems against pathogens and tumors (2, 8, 18). It has been reported that one of the major safety advantages of MVA is that it develops an incomplete morphogenetic pathway in human cells (7, 8, 53). Therefore, the infection of human cells with MVA is not expected to produce mature and infectious particles. In addition, MVA contains large deletions in the genome (3) which affect genes that counteract host immune responses (4). The threat of bioterrorism with variola virus has potentiated the use of MVA as a vaccine against smallpox, since it avoids the complications in immunosuppressed individuals that occur with the current VV vaccine.

The morphogenesis of VV is a very complex process that has been extensively analyzed by electron microscopy (12, 15, 19, 20, 22, 26, 30, 37, 43–45). Once VV has entered the cell, uncoating and release of viral particle components takes place (25). The first evidence for virus assembly is the crescent-shaped membranes, which surround electron-dense areas or viroplasm foci (9, 10, 12, 31). These large structures are called

\* Corresponding author. Mailing address: Department of Molecular and Cellular Biology, Centro Nacional de Biotecnología, Campus Universidad Autónoma, 28049 Madrid, Spain. Phone: 34-91-585-4503. Fax: 34-91-585-4506. E-mail: mesteban@cnb.uam.es.

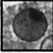

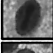
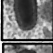
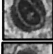

	WR	MVA	ANKARA	NYCBH
	<b>40.9</b>	<b>63.5</b>	<b>63</b>	<b>84</b>
	<b>9.3</b>	<b>3.1</b>	<b>5</b>	<b>5</b>
	<b>17.6</b>	<b>3.8</b>	<b>22</b>	<b>4.5</b>
	<b>6.5</b>	<b>3.1</b>	<b>3.5</b>	<b>1</b>
	<b>1.3</b>	<b>25.5</b>	<b>0.5</b>	<b>2.5</b>
	<b>24.1</b>	<b>0.7</b>	<b>6</b>	<b>3</b>

FIG. 1. Quantification of viral forms (percentage) produced in HeLa cells infected for 12 h with different VV strains—WR, MVA, Ankara, and NYCBH. More than 400 particles were counted per sample, as described in Materials and Methods.

viral factories and represent the sites for viral replication and assembly of the first immature spherical form. In these areas several elements are cooperating, such as microtubules with RNA and viral proteins (21, 28, 32, 41, 47), and vimentin intermediate filaments with ERGIC membranes and viral proteins (VV core protein, p39) for assembling the new immature viral forms (IVs) (19, 37, 51). The IVs undergo additional maturation events, transforming into brick-shaped structures where the envelope surrounds an electron-dense core structure containing the viral DNA. These virions constitute the first infectious form of the virus and are referred to as intracellular mature virus (IMV). A small portion of IMVs become wrapped by a membrane cisternae derived from the trans-Golgi network to form the intracellular envelope virus (IEV), and they are released from the cell by fusion with the plasma membrane. The extracellular envelope virus (EEV) are largely responsible for virus spread (for a review, see reference 50).

It is becoming clear that the complex VV morphogenesis process implies a number of components of the host cell, such as organelles and motor and other functional proteins. The wrapping and disassembly of the endoplasmic reticulum around the viral DNA replication site may occur in analogy to nuclear envelope dynamics during cell cycle (54). Recently, several groups have found the participation of microtubules in different steps of the morphogenetic pathway. Some IMVs are transported from the factory on microtubules to sites of wrapping with intracellular membranes to form the IEV. This virus then moves via microtubules to the cell surface, where the outer membrane fuses with the cell plasma membrane, leaving a virus particle with three membranes in the cell surface, and this viral form, referred as CEV actin tails, appears to be responsible for the projection of the CEV to neighboring cells and activates the cell-to-cell spreading process (for a review, see reference 50). There are several studies concerning cytoskeleton alteration with the wild type and with other mutant strains, but little is known about the effects of MVA in the host cell.

The ability of MVA to activate strong cellular immune responses after expression of foreign antigens has been related to deletions of virus genes encoding immunomodulatory molecules, which in a wild-type virus background provide a selective

advantage to counteract host immune responses (1, 4). Since MVA maturation has been reported to be inhibited at the IV formation stage in human cells (7, 8, 46, 53), it is possible that other factors might contribute to the good activation of immune responses by MVA recombinants.

In this report, we have used confocal and electron microscopy approaches to carry out a detailed characterization of MVA-induced morphological changes of human cells and identification of viral intermediates during the virus maturation process, in comparison with cells infected with other strains of VV (wild-type Western Reserve [WR], Ankara, and New York City Board of Health [NYCBH]). We show that in HeLa cells MVA triggers morphological changes and produces viral forms that differ from cells infected with the other VV strains.

#### MATERIALS AND METHODS

**Cells and viruses.** African green monkey kidney cells (BSC-40) and human HeLa cells were grown in Dulbecco modified Eagle medium, supplemented with 10% newborn bovine serum. Baby hamster kidney cell (BHK-2) and primary chicken embryo fibroblast (CEF) cells were grown in the same medium but supplemented with 10% fetal bovine serum. The VV strains used in this work, the WR strain, MVA obtained after 575 passages in CEFs, and its parental Ankara strain (both strains kindly provided by Gerd Sutter, Munich, Germany) and the NYCBH strain (kindly provided by B. Moss), that is the component of DryVax used in the USA and in many other countries as a vaccine against smallpox, were propagated and titrated in BSC-40 cells (WR, Ankara, and NYCBH) or in BHK-21 or CEFs for MVA. All viruses were purified by banding after sucrose gradient centrifugation (43, 45).

**One-step virus growth and virus titration by immunostaining.** To study the growth dynamics of MVA in comparison with the WR strain, monolayers of HeLa cells were infected with viruses at 5 PFU/cell (PFU). After binding at 4°C for 1 h, monolayers were washed three times with phosphate-buffered saline (PBS) and, at 0, 3, 6, 12, 18, and 24 h postinfection (hpi), medium samples were collected, and the cell monolayer was also harvested by scraping and centrifugation. The cells were lysed by three cycles of freezing and thawing, and the supernatant was recovered and stored frozen. Virus titers were determined by immunostaining on BSC-40 cells for the WR strain and on BHK-21 cells for MVA. At 24 hpi the infected monolayers were washed three times with PBS, fixed, and permeabilized with methanol-acetone (1:1) for 5 min at room temperature and incubated for 30 min at 37°C with a rabbit anti-VV polyclonal antiserum diluted 1:1,000 with PBS containing 3% fetal calf serum. After one wash with PBS, the monolayers were incubated with a secondary antibody (goat anti-rabbit antibody conjugated with peroxidase) under the conditions described above for primary antibody. The plaques in infected cells were revealed with PBS

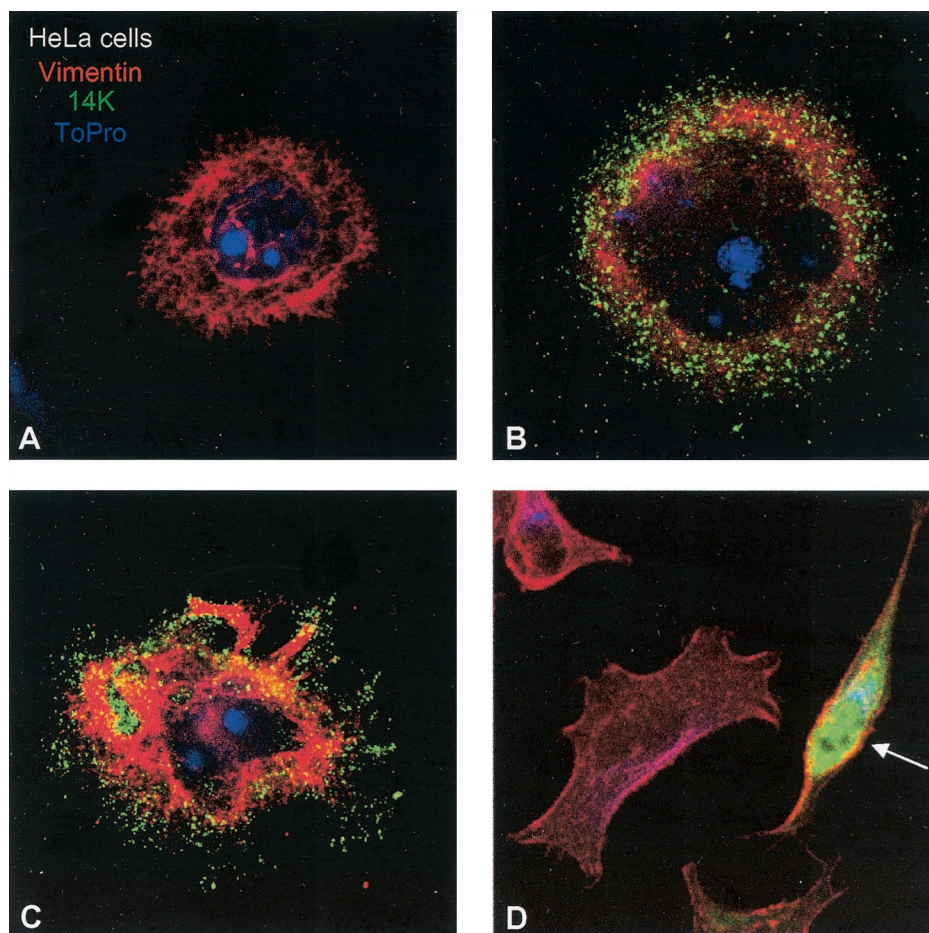


FIG. 2. Differential morphological changes induced in epithelial HeLa cells after infection with the WR and MVA VV strains. HeLa cells were infected with WR and MVA at 0.05 PFU/cell, and at 48 hpi cells were fixed with paraformaldehyde, glutaraldehyde, and Triton X-100 in CB. Soluble cytoplasmic p14 viral protein and virions were detected with an antibody to the p14 protein (A27L gene) of VV and a secondary antibody conjugated with FITC; the cellular cytoskeletal vimentin was detected with a monoclonal antibody and a secondary antibody conjugated with TRITC (tetramethyl rhodamine isothiocyanate); the DNA was visualized by staining with To-Pro. More than 50 fields at  $\times 40$  magnification were captured, and the changes in the morphology of infected cells were registered and quantified (not shown). (A) Mock-infected cell. (B and C) Cells infected with WR, exhibiting a rounded and multipolar morphology. (D) MVA-infected cell with a characteristic bipolar morphology (arrow).

containing diaminobenzidine. Although there is a major restriction in the replication of MVA compared to HeLa cells infected with WR, the shape of the growth curve indicates the production of some infectious virus particles (data not shown), in agreement with other reports (4, 7).

**Electron microscopy.** (i) **Negative staining of purified virions.** Sucrose-purified WR, Ankara, NYCBH, and MVA virions were adsorbed to electron microscopy grids coated with collodion and carbon and made hydrophilic by glow discharge. After a wash in distilled water, samples were stained with a 2% solution of uranyl acetate for 30 s, allowed to dry, and analyzed by transmission electron microscopy (38).

(ii) **Embedding of infected cells in EML-812.** Monolayers of HeLa and CEF cells were infected at a multiplicity of infection (MOI) of 5 PFU/cell with the VV strains WR, Ankara, NYCBH, or MVA. At 6 and 12 hpi, cells were fixed in situ with a mixture of 2% glutaraldehyde and 1% tannic acid in 0.4 M HEPES buffer (pH 7.5) for 1 h at room temperature. Fixed monolayers were removed from the culture dishes in the fixative and transferred to Eppendorf tubes. After centrifugation and a wash with HEPES buffer, the cells were stored at 4°C until use.

For ultrastructural studies, fixed cells were processed for embedding in the epoxy resin EML-812 (TAAB Laboratories, Ltd., Berkshire, United Kingdom) as previously described (38). Postfixation of cells was done with a mixture of 1% osmium tetroxide and 0.8% potassium ferricyanide in distilled water for 1 h at 4°C. After four washes with HEPES buffer, samples were treated with 2% uranyl acetate, washed again, and dehydrated in increasing concentrations of acetone (50, 70, 90, and 100%) for 10 min each time at 4°C. Infiltration in resin was done

at room temperature for 1 day. Polymerization of infiltrated samples was done at 60°C for 3 days. Ultrathin sections (20 to 30 nm thick) of the samples were stained with saturated uranyl acetate and lead citrate by standard procedures. Collection of images from negative staining and ultrathin sections were done in a JEOL 1200-EX II electron microscope operating at 100 kV (31, 37–40).

**Quantitative analysis of viral forms by electron microscopy.** Approximately 75 infected cells per sample were studied. The results are expressed as the percentage that each intermediate represents in the total of viral particles quantified for a particular sample. A total of 2,344 viral particles (>400 particles per sample) were studied and are included in Fig. 1.

**Immunofluorescence microscopy.** To define the subcellular distribution of viral proteins and the alterations produced in the cytoskeletal network of the host cell, HeLa and BSC-40 cells grown to near confluency on coverslips were infected at an MOI of 0.05 PFU/cell with the VV strains WR, Ankara, NYCBH, or MVA. At late times (24 and 48 hpi) the infected cells were fixed. Two fixation procedures were applied. For conventional studies, a mixture of 3.8% paraformaldehyde, 0.2% glutaraldehyde, and 0.05% Triton X-100 in PBS was used. To evaluate the alteration at cytoskeleton (production of actin tails), BSC-40 cells were infected at an MOI of 1 PFU/cell and were fixed at 18 hpi. To detect delicate elements of the cytoskeleton in fixed cells, we used cytoskeletal buffer (CB) with some modifications. CB is composed of 10 mM morpholineethanesulfonic acid (MES), 150 mM NaCl, 5 mM EGTA, 5 mM MgCl<sub>2</sub>, and 5 mM glucose (pH 6.1) (9, 29). The fixation was done at 37°C for 30 min, and samples were stored in CB at 4°C until use. After a wash in CB, cells were permeabilized with CB containing

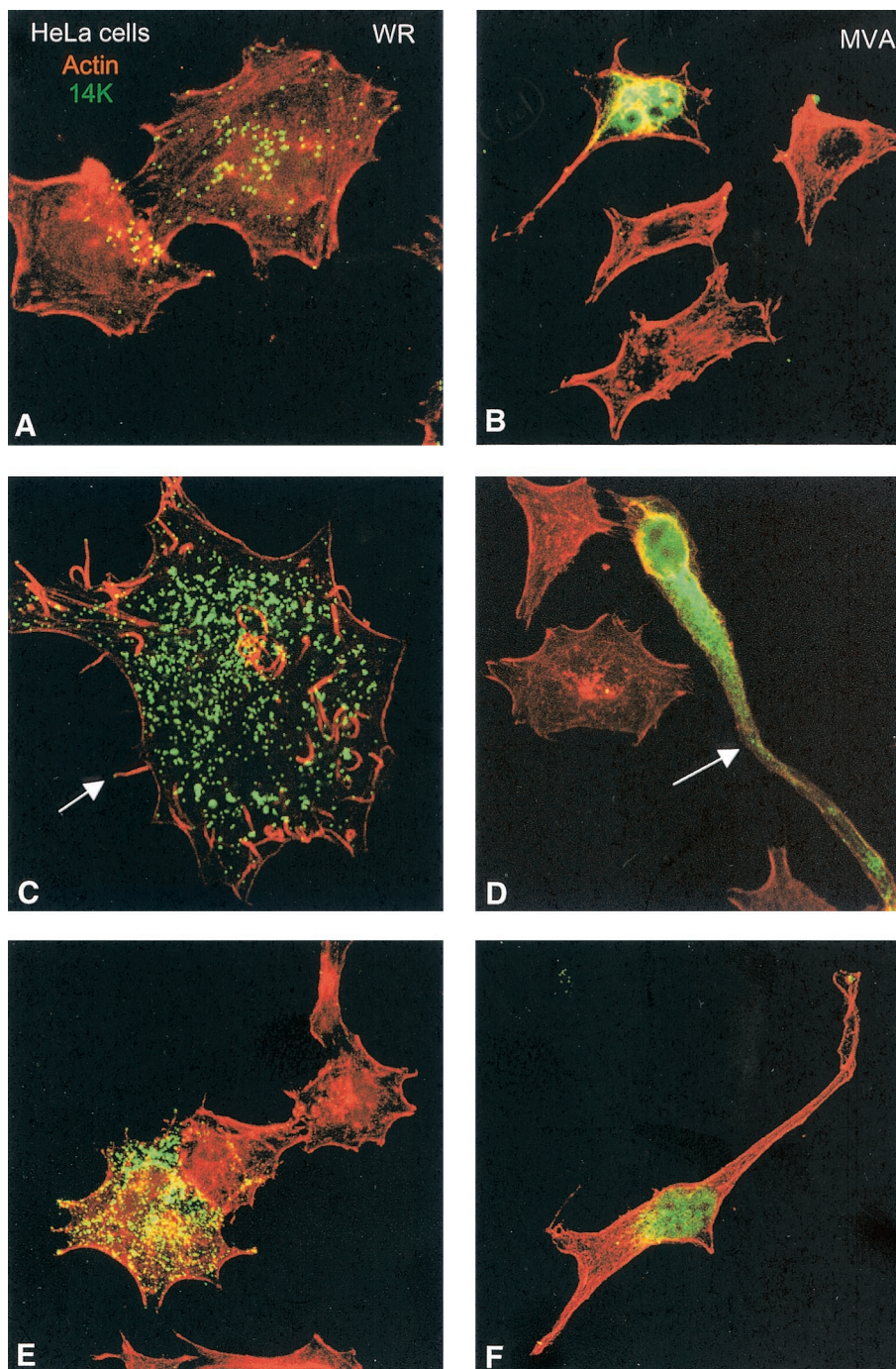
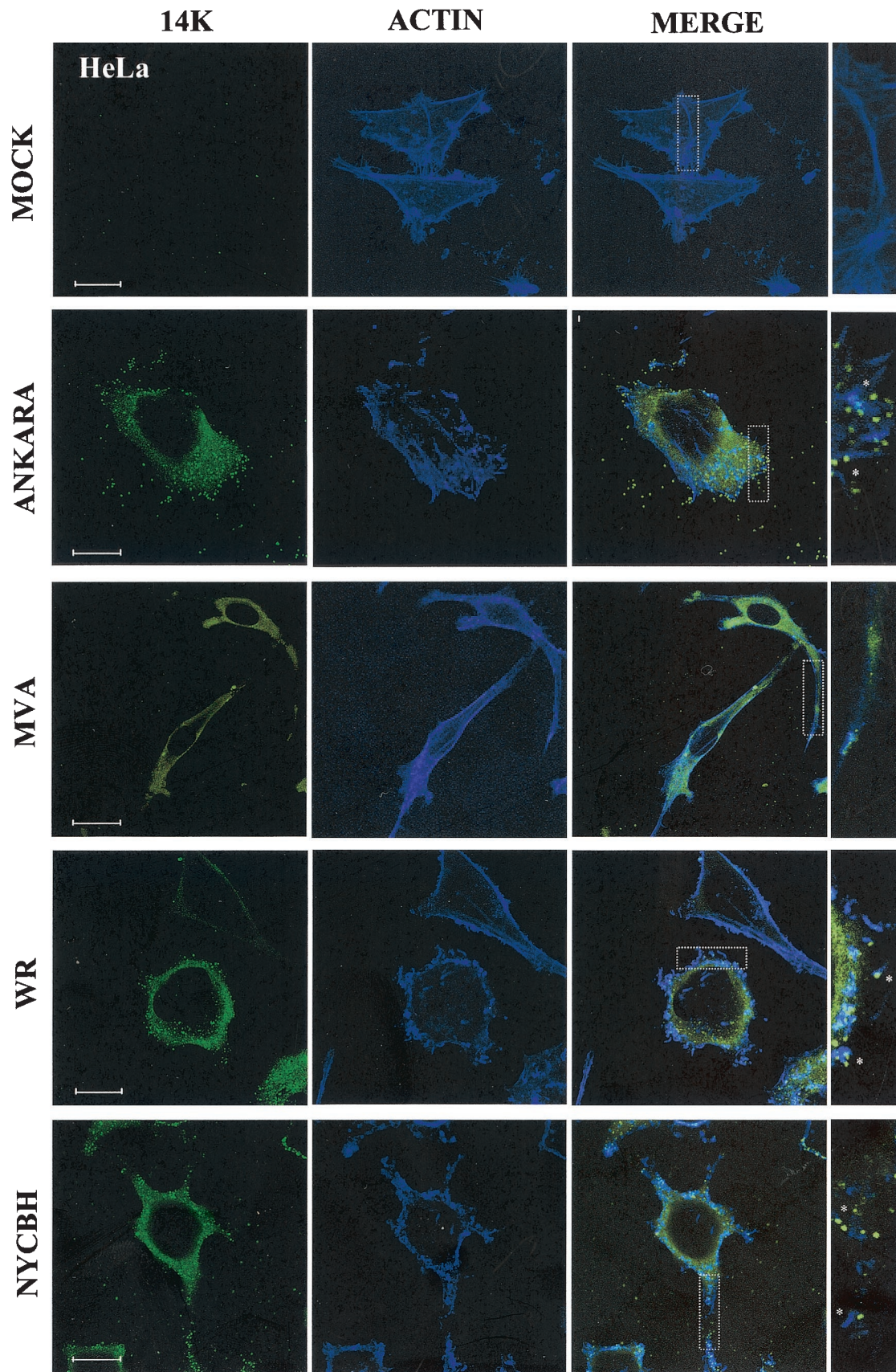


FIG. 3. Distinct cell polarization and actin tails in HeLa cells infected with MVA compared to the WR strain. HeLa cells were infected with WR and MVA at 0.05 PFU/cell, and at 48 hpi cells were fixed and processed for confocal microscopy. Cytoplasmic viral p14 protein and virions were detected with an antibody to p14 protein and a secondary antibody conjugated with FITC; cellular actin was detected with phalloidin conjugated to TRITC. In cells infected with WR, individual virions (A, C, and E) and actin tails (arrow in panel C) are clearly seen in these Z-projections. The morphology of these infected cells is multipolar or stellated. Cells infected with MVA (B, D, and F) produced few virions (one is indicated by an arrow in panel D) and showed a bipolar morphology, and actin tails were not induced.

0.5% Triton X-100. Coverslips were then blocked for 30 min with a solution of CB containing 2% fetal bovine serum and 0.05% Triton X-100 (wash/blocking solution). Cells were incubated for 30 min at 37°C with an antibody diluted in wash/blocking solution: the mouse monoclonal MAb.C3 or rabbit polyclonal antibody directed against the membrane p14 protein (A27L gene) of VV. The coverslips were then extensively washed with CB, followed by incubation in

darkness for 30 min at 37°C, with anti-mouse secondary antibody conjugated with fluorescein isothiocyanate (FITC), with phalloidin conjugated with rhodamin (Sigma), and with the DNA staining reagent To-Pro (Molecular Probes). The cells were washed with CB and postfixed to stabilize the fluorescence, and the coverslips were mounted by using Mowiol containing 0.2% DABCO (Sigma) as an antifading agent. Images were obtained by using a Bio-Rad Radiance 2100



confocal laser microscope, and the images were collected by using Lasersharp 2000 software and processed in Adobe Photoshop 6.0.

## RESULTS

### Infection of epithelial cells with MVA produces bipolar cells.

It is unclear if the consequences of MVA infection on cells are the same as those triggered by other strains of VV. Thus, we compared the morphological changes induced in cultured cells by infection with MVA versus those induced by the VV strain WR, since this is the most widely studied virus strain. To analyze the effect of MVA infection, epithelial cells were infected at a low MOI to minimize the effect of the virus in the cell monolayer and to visualize the morphology of single infected cell, as well as the process of virus spreading to neighboring cells. Epithelial cells (BSC-40 and HeLa cells) were infected with MVA or WR strains at 0.05 PFU/cell, and cells were fixed at late times postinfection. Cytoskeletal elements (actin and vimentin) were labeled, together with an antibody to the viral envelope protein p14 (A27L gene). As determined by confocal microscopy at 48 hpi, the epithelial HeLa cells infected with WR strain were multipolar and have rounded morphology (Fig. 2C and D). In contrast, MVA infection produces bipolar cells (Fig. 2E). Quantification of more than 50 fields at a magnification of  $\times 40$  for each strain of VV showed that WR produces 73.2 and 21.4% of the multipolar and rounded cells, respectively, and only 5.4% of these cells were bipolar. The same quantification for MVA showed that 68.5% of the infected cells were bipolar or elongated, 27.8% were multipolar or stellated, and only 3.7% were rounded.

To get a more detailed quantification of the morphological changes produced in infected cells, we evaluated the ability of the infected cells to induce the formation of cellular projections as described for the WR strain, a phenomenon that requires the expression of late viral genes (47, 48). Cells infected with WR strain had three to five projections (75.5%), and only 6.7% had two projections, showing that most of them are multipolar or stellated cells. In comparison, 51% of cells infected with MVA had two projections per cell, and 44% of them had three to five projections, and bipolar cells were more frequently observed than multipolar cells. The length of the projections was smaller for cells infected with WR strain compared to cells infected with MVA. That is, 93.2% of WR-infected cells had a projection length 0.2 to 0.5 times the length of the cellular body, whereas 86.3% of the MVA-infected cells had a projection length of 0.5 to 2 cellular bodies.

The morphological alterations of infected cells were further analyzed by labeling the actin cytoskeleton and the virions. Infection of HeLa cells with WR generated, at 48 hpi, many virions and a small amount of nonassembled viral p14 cytoplasmic protein. Most of the viral p14 protein is incorporated

into mature virions (Fig. 3A, C, and E). The infected cells conserved the described phenotype (multipolar or stellated). Infection with WR induces actin tails and microvilli, and virus particles at the ends of these structures are visible (Fig. 3C). However, infection of HeLa cells with MVA accumulated largely cytoplasmic p14 viral protein, with apparently few virions (Fig. 3D). MVA-infected cells did not show actin tails or microvilli but did undergo a reorganization of the cytoskeleton. Bipolar cell morphology is generated in MVA-infected cells, in comparison with surrounding healthy cells (Fig. 3B, D, and E).

The data of Fig. 2 and 3 revealed that infection of epithelial HeLa cells with MVA produces bipolar cells that acquire long and branching projections, whereas infection with WR strain produces multipolar and rounded cells with few branches. Most of the p14 viral protein is incorporated into virions in WR strain-infected cells, a finding clearly distinct from MVA-infected cells, in which few virions appeared to be produced.

**MVA-induced polarization in epithelial cells is distinct from cells infected with VV strains Ankara and NYCBH.** To document whether the morphological changes induced by MVA were the same as or different from those induced by its parental strain and by other VV strains, we carried out an analysis by confocal microscopy of HeLa cells infected with MVA, with its parental strain Ankara, and with the other VV strains WR and NYCBH. For these experiments actin was labeled in blue, and the virus was labeled in green. As shown in Fig. 4 with actin staining, whereas MVA induced the characteristic bipolar morphology, cells infected with the parental Ankara virus had a stellated morphology similar to that of cells infected with the WR strain. Cells infected with NYCBH strain also had an stellated morphology but contained more projections. After being stained the cells with an antibody to the virus envelope protein p14, virions were readily observed in cells infected with the WR and Ankara strains but were less abundant in cells infected with NYCBH. However, in cells infected with MVA, most of the label was cytoplasmic, with very few virions present. Under conditions that visualize the actin tails, we observed label virions on the tip of an actin tail in cells infected with the WR and Ankara strains but reduced in numbers in cells infected with NYCBH. A magnified area of cells with actin tails and virions is shown to the right side of the images in Fig. 4. It should be noted that CEVs are found at the ends of actin tails (50), but the use of detergent after fixation of cells does not allow differentiation of the different viral forms with the p14 antibody.

To evaluate further the epithelial morphological changes in virus-infected cells, we visualized by confocal microscopy the progression of infection at low MOI, comparing (MVA and WR strains), by using BSC-40 cells fixed at 48 hpi. We selected BSC-40 cells for these studies because this is a primate cell line

FIG. 4. Differences in virus-induced polarization and actin tails between HeLa cells infected with MVA, its parental Ankara strain, and the other VV strains, WR and NYCBH. HeLa cells were infected with the MVA, Ankara, WR, and NYCBH VV strains at 0.05 PFU/cell, and at 48 hpi cells were fixed and processed for confocal microscopy. Cytoplasmic viral p14 protein and virions were detected with an antibody to p14 protein and a secondary antibody conjugated with FITC; cellular actin was detected with phalloidin-conjugated with Far Red. In cells infected with the Ankara, WR, and NYCBH strains there is a multipolar or stellated morphology and actin tails are clearly seen in these Z-projections. In mock-infected cells the F-actin is present in fibers. However, cells infected with MVA showed a bipolar morphology, actin tails were not induced, the cells accumulated cytoplasmic p14 viral protein, and very few virions were observed. Bar, 1  $\mu\text{m}$ .

described as semipermissive for MVA maturation (7) and has clearly distinguishable intercellular junctions and cytoskeleton. In addition, BSC-40 cells are the most commonly used cell line for VV titration since they form plaques in liquid overlay and comets during virus spreading. Infection of cells with WR at a low MOI (0.05 PFU/cell) gives a characteristic virus plaque (Fig. 5A), where cells become motile and pull apart (48, 49). However, in MVA-infected cells there is no plaque but rather a cluster of infected cells (Fig. 5B). This suggests that a single infected cell is able to spread the infection to the surrounding cells, both for WR and MVA. A closer look shows that in WR-infected cells, virions are abundant and account for most of the p14 protein labeling (Fig. 5C and E). These mature viruses are observed during exit from the cell and spread to neighboring cells (Fig. 5E, arrow). In MVA-infected cells, the cytoplasm of the cell is heavily stained with p14 viral protein, and virions are very scarce. The MVA-infected cells connect themselves to other cells by using a long phillipodium (Fig. 5D and F). The final product of this process is the foci of infection that produces the characteristic plaque phenotype of MVA: a group of infected cells (ca. 20 to 30) (Fig. 5B), surrounded by healthy cells with well defined actin stress fibers (Fig. 5F, arrow). A closer examination of actin fibers in BSC-40 cells infected with MVA failed to reveal the characteristic coiled actin tails. This was confirmed by a comparison of actin fibers from BSC-40 cells infected with the different VV strains, MVA, Ankara, WR, and NYCBH. After the cells were stained for actin and virions for p14, as indicated in Fig. 4, we found actin tails with virions on the tips in cells infected with the WR, Ankara, and NYCBH strains but not in cells infected with MVA (data not shown).

**Differences in the morphogenetic pathway between MVA and other VV strains (WR, Ankara, and NYCBH) in virus-infected human cells.** It has been previously described that human cells infected with MVA result largely in the accumulation of IV forms with no production of mature viral forms (7, 8, 46, 53). Since the confocal experiments described in Fig. 2 to 4 indicate that few mature viral forms might be assembled in MVA-infected human cells, we carried out an in-depth analysis by transmission electron microscopy of the viral forms produced in the course of infection of HeLa cells. We compared the viral forms produced in cells infected with MVA versus WR, Ankara, and NYCBH. We used cultured cells (HeLa and CEF) infected for 6 and 12 h to visualize intermediates in the virus assembly process. The most relevant ultrastructural findings of morphogenesis in cells infected with WR, Ankara, NYCBH, and MVA are described as a sequence of steps (Fig. 6 to 9). We present the intermediate viral forms found in HeLa cells infected with WR in Fig. 6, the viral forms observed in CEF cells infected with MVA in Fig. 7, the viral forms found in HeLa cells infected with MVA in Fig. 8, and the viral forms in HeLa cells infected with Ankara and NYCBH strains in Fig. 9. The electron microscopy studies revealed that the main viral forms described for strains WR, Ankara, and NYCBH in HeLa cells are detected in MVA-infected CEF cells, although there are differences in fine ultrastructure, especially in the case of IMVs. The IMVs produced in MVA-infected cells exhibit a more rounded shape than those from the WR, Ankara, and NYCBH strain-infected cells (compare Fig. 6B and H and Fig. 9A and D with Fig. 7B and Fig. 8C and F). This was confirmed

after negative staining of sucrose-purified IMVs obtained from BHK-21 cells, which are permissive for the MVA, Ankara, WR, and NYCBH strains. The dimensions and heterogeneity of viral particles from the four VV strains, with ca. 50 viral particles measured per viral strain, are shown in Fig. 10. Virions from WR have the typical brick shape, with 6% of the particles rounded, and with an average size of  $310 \pm 11$  nm by  $252 \pm 16$  nm. Virions from Ankara also have a typical brick shape, with 7.4% rounded and with dimensions of  $305 \pm 16$  nm by  $262 \pm 16$  nm. Virions from NYCBH showed different shapes, with 72.5% with a brick shape, 22.5% with a narrow brick shape (a representative is shown on the right of panel C), and 7.5% with a rounded shape (with dimensions of  $303 \pm 15$  nm by  $241 \pm 25$  nm). Similar preparations of purified MVA showed a considerable percentage of rounded particles (48%), with an average size of  $296 \pm 62$  nm by  $253 \pm 18$  nm.

A closer electron microscopy examination of HeLa cells infected with strains WR (Fig. 6B to J), Ankara and NYCBH (Fig. 9), and MVA (Fig. 8B to H) revealed clear differences in the accumulation of intermediates of virus maturation, and the results of a quantitative analysis of the various viral forms at 12 hpi are presented in Fig. 1. The viral forms observed are genuine intermediates of MVA replication since their numbers increase with time. In agreement with the electron microscopy findings of others (7, 8, 46, 53), the main restriction of viral forms in HeLa cells infected with MVA is at the level of progression from IV forms, since this is the most abundant viral form (63.5%). In addition to the well-characterized viral forms previously described (19, 51), we find in cells infected with the various VV strains a viral form that probably represents a “transition” between IV and IMV and has been described as an occasional stage by Carroll and Moss (7). This intermediate of maturation is electron dense and has a spherical form, with an average diameter of 200 nm (Fig. 6E, 7D, and 9D). The “transition form” is able to take an additional envelope (Fig. 6F, 7E, and 8E). The transition forms were found occasionally outside of the cell (Fig. 7I). A viral form in the process of construction of the internal viral core (Fig. 6G), previously described for WR (51), was also observed in MVA and NYCBH-infected HeLa cells (Fig. 8C and 9C). Although the core structure can be recognized, it seems that the core has not been completely “sealed” to the envelope. Some viral forms reached the IMV stage in MVA- and NYCBH-infected HeLa cells (Fig. 8G and 9D), and some of them are seen wrapped by a second envelope (Fig. 8H).

Although the main viral forms described for WR and Ankara are detected in MVA-infected cells (both under permissive and nonpermissive conditions), there are important differences both in fine ultrastructure and in the amounts of the intermediates compared to cells infected with the strains WR and Ankara (Fig. 1). First of all, some MVA particles reached the mature IMV form, but IMVs produced in MVA-infected cells exhibited a more rounded shape, as seen both in thin sections of infected cells (Fig. 7 and 8) and after negative staining of isolated viruses (Fig. 10). In addition, when MVA infects HeLa cells, IMVs have an abnormal internal structure (“atypical” viruses) with potential alterations in the interactions core envelope (Fig. 8C and F). On the other hand, these “IMVs,” which are frequently found (25.5%) in MVA-infected HeLa cells (Fig. 1), are not able to efficiently acquire the

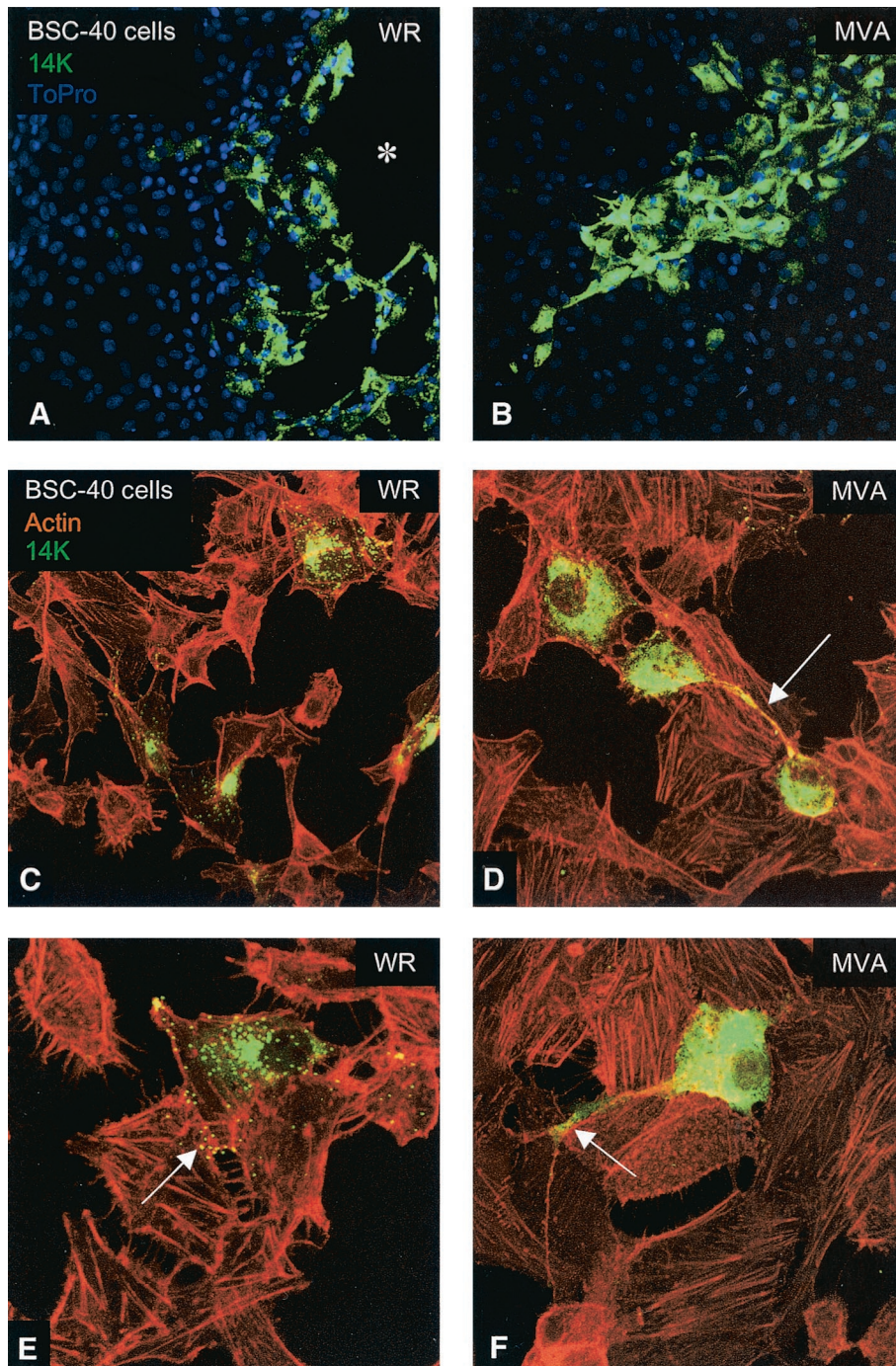


FIG. 5. Monkey cells infected with MVA accumulate cytoplasmic viral protein with few virions, do not produce actin tails, and generate filopodia. Monolayers of BSC-40 cells were infected with WR or MVA at 0.05 PFU/cell and, 48 h later, cells were fixed and processed by a method that adequately preserves the cytoskeleton. Cytoplasmic viral p14 protein and virions were detected with anti-p14 antibody and a secondary antibody conjugated with FITC. Actin was detected with phalloidin conjugated with TRITC, and DNA was labeled with To-Pro. The upper panels showed the virus plaques produced by WR (asterisk in panel A) and by MVA. In panel C there are four WR-infected cells without connections between them, while in panel D the cells infected with MVA show a filopodium (arrow in panel D) connecting two cells. At higher magnifications (E and F), it is clear that WR strain-infected cells produced virions that exit the cells (arrow in panel E) and spread to the neighboring cells. In comparison to cells infected with strain WR, MVA-infected cells produced very few virions and a larger amount of cytoplasmic p14 viral protein, and some cells generated a long filopodium (arrow in panel F). Whereas actin tails were found in cells infected with strain WR, no such tails were observed in MVA-infected cells.



WR VV/HeLa

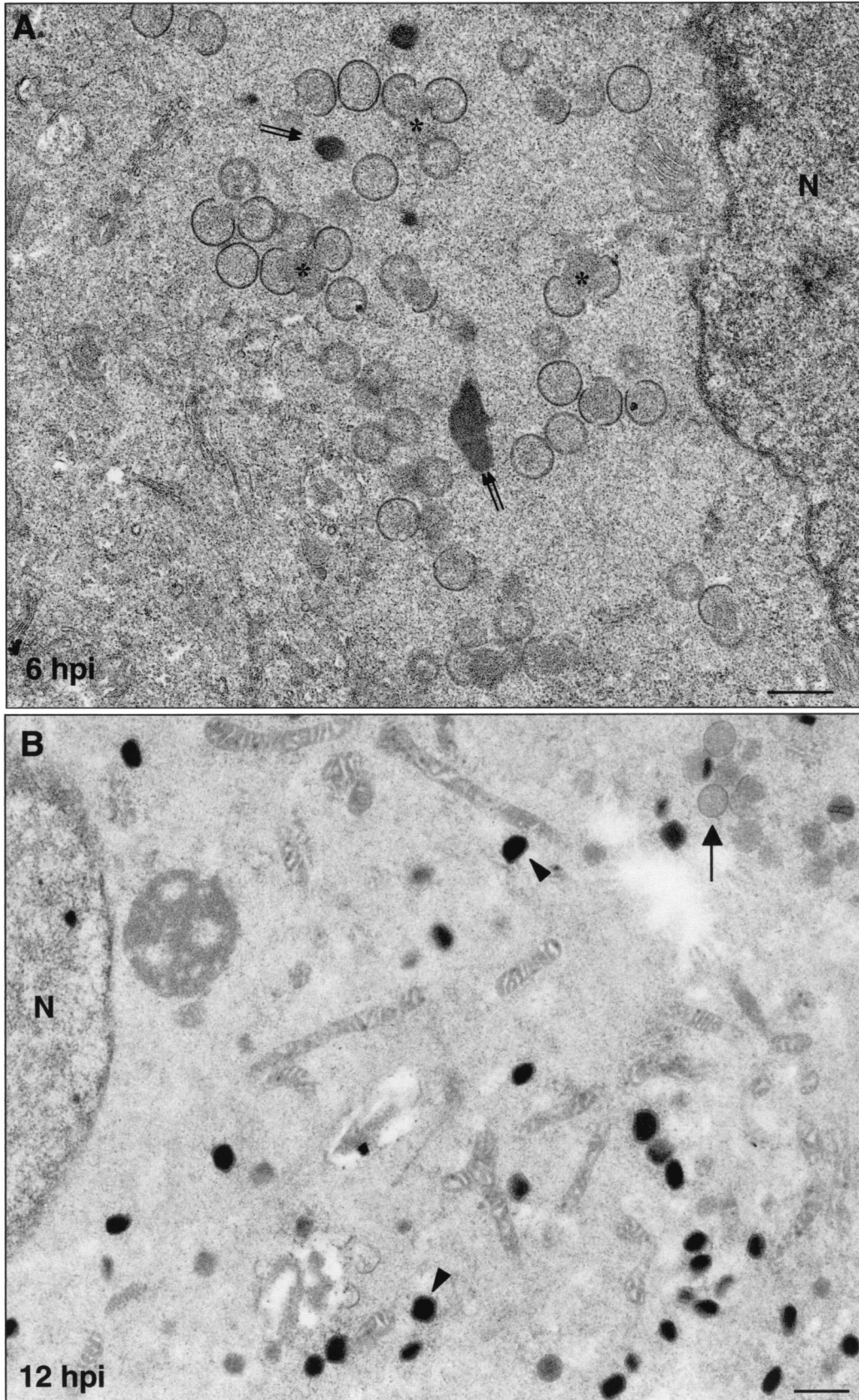


FIG. 6

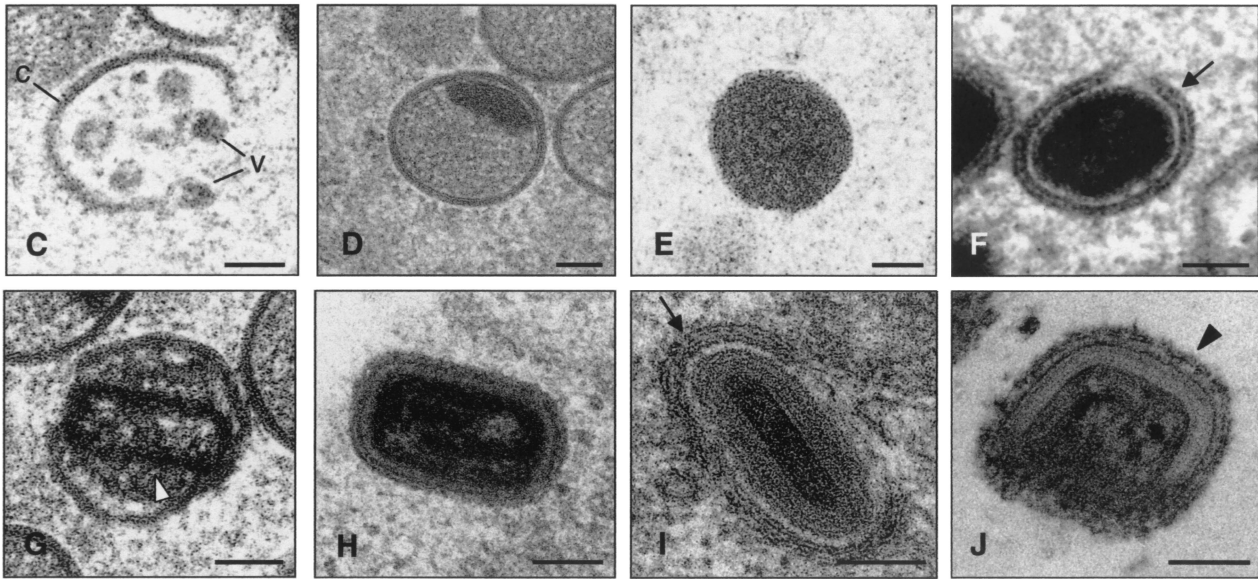


FIG. 6. Viral forms produced in human cells infected with strain WR as visualized by electron microscopy. Monolayers of HeLa cells infected at 5 PFU of virus/cell were chemically fixed at 6 and at 12 hpi and then processed for conventional embedding in an epoxy resin. Ultrathin sections were studied by transmission electron microscopy at both low and high magnifications. (A) At 6 hpi small viroplasm foci and forming viruses (asterisks) were detected near the nucleus (N) of infected cells. DNA crystalloids of variable size (double arrow) were also frequent in the assembly areas. (B) At 12 hpi the IMVs (arrowheads) were the predominant viral form. A minor population of IVs was also observed (arrow). (C to J) The hypothetical sequence of morphogenesis of the WR strain of VV is shown at higher magnifications. (C) Viral crescent (c) with associated vesicular (v) elements; (D) characteristic IV with DNA spot; (E) previously proposed spherical and dense transition form IV→IMV. This viral form is occasionally seen being wrapped by two membrane units, as shown in panel F (arrow). (G) Potential intermediate in the process of core assembly (arrowhead). Characteristic mature forms are shown in panels H to J: IMV (H), IEV (I; the arrow points to the additional double membrane), and EEV (J; the arrowhead points to the thick external coat). Bars: 0.5  $\mu$ m, A and B; 100 nm, C to J.

additional double envelope to become IEVs, since “IMVs” attached to intracellular membranes are seen but not totally wrapped by them (Fig. 8). In the case of HeLa cells infected with strain NYCBH, we find a large proportion of viral forms as IVs (84%) dispersed in the cytoplasm, some of them surrounded with dense membranes, and few IMVs (Fig. 1 and 9). NYCBH produces fewer “atypical” IMVs than MVA. The presence of potential CEVs was very scarce in HeLa cells infected with MVA (Fig. 1). In conclusion, although in HeLa cells MVA is able to reach the “IMV” stage, these virions were not structurally normal, and the subsequent steps in the morphogenetic pathway are clearly blocked.

## DISCUSSION

We have used confocal and electron microscopy approaches to provide a detailed characterization of the morphological changes induced in HeLa cells by MVA and of the different viral forms produced in the course of the virus infection. These analyses have been compared to cells infected with the parental Ankara strain and with other VV strains, i.e., WR and NYCBH. In this work, we present new findings on cell polarization triggered by MVA and describe the different viral forms produced in human cells.

According to confocal microscopy analysis, MVA infection has a different impact in HeLa cells compared to infection with the WR, Ankara, and NYCBH strains (Fig. 2 to 4). Infection with MVA leads to a distinct change in cell morphology, and

the alterations are remarkable, since the cells become polarized or have an elongated shape with two poles (bipolar).

It is traditionally considered that MVA produces minimal cytopathic effects in human cells compared to infection with the WR strain (8). This is clear when immunostained cells are observed by light microscopy (7, 14). These morphological alterations produced by MVA might not be anecdotal since they might be used to establish connections with neighboring cells. Certainly, we have observed numerous fields by confocal microscopy where these MVA-induced cellular projections connect with other cells, where infection is starting (Fig. 5). The morphological changes in the epithelial cells are better observed at a low MOI, when it is easy to visualize the virus spread. When cells are infected at high MOI the polarization process is hidden because the virus polarizes several cells in distinct orientations and, therefore, the unidirectional spread of the virus is eliminated. Under these conditions, it is still possible to observe the bipolar cells at the periphery of a focus of infection. Although the WR and Ankara strains have equal probabilities to exit the cell in all directions, causing the stellated phenotype (Fig. 4), MVA has limited ability to exit the cell and, therefore, it has a better chance to polarize the host cell. By infecting HeLa cells at a high MOI, the binding to cells of virions activate a signal cascade that generates protrusions in the plasma membrane that can be essential for virus entry (21). Using a low MOI and long times postinfection (2 days), we observed similar protrusion, which indicates that cytoskeletal changes occur both during entry and exit of the virus from

## MVA VV/CEF

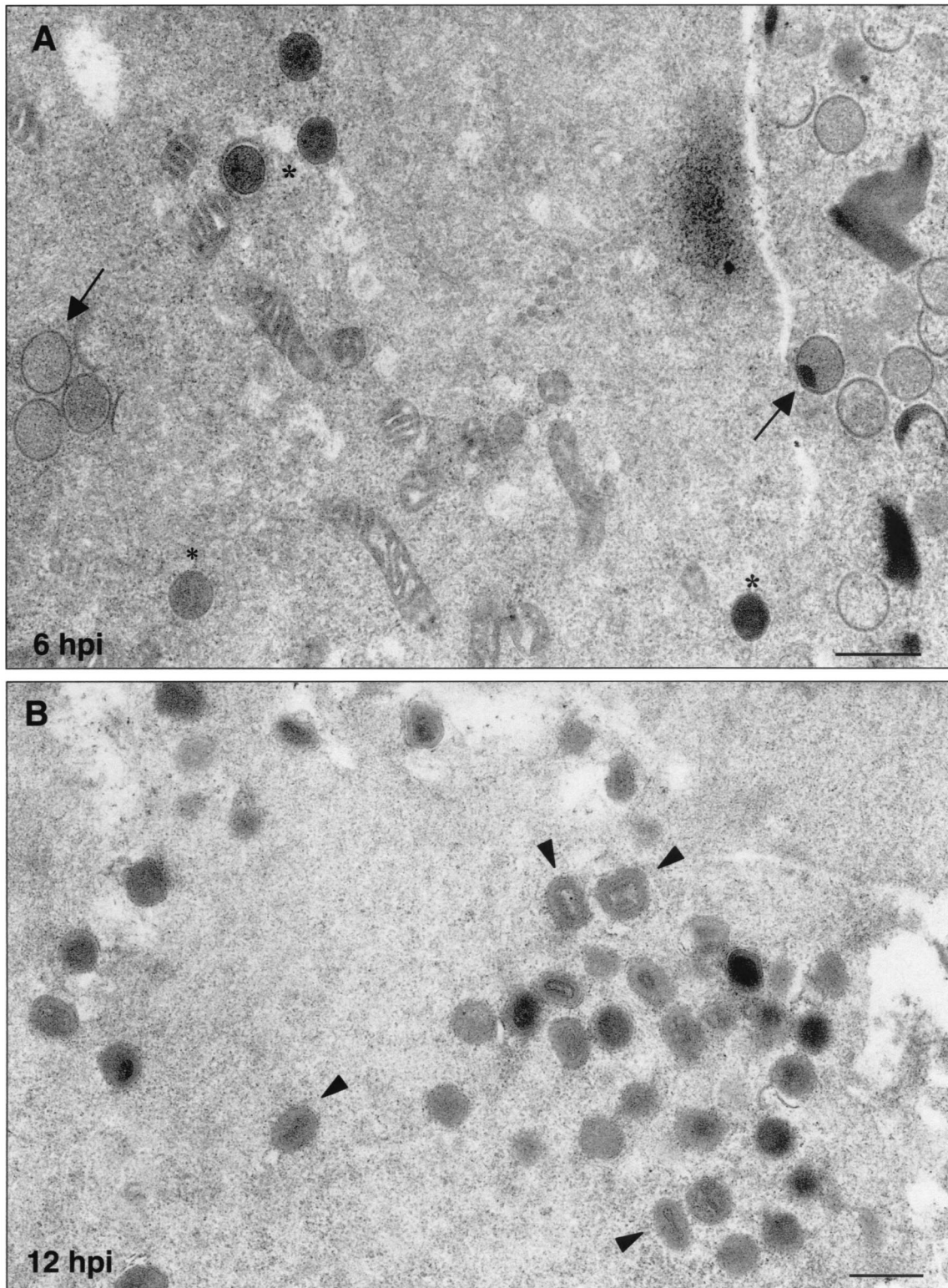


FIG. 7. Morphogenetic events in CEFs infected with MVA. Primary CEFs infected at an MOI of 5 PFU/cell were chemically fixed at 6 and 12 hpi and processed for conventional embedding in an epoxy resin. Ultrathin sections were studied by transmission electron microscopy at low and high magnifications. (A) At 6 hpi, IVs (arrows) and spherical and dense transition forms (asterisks) were abundant. (B) At 12 hpi, IMVs constituted the most abundant viral form (arrowheads). Also, a DNA crystalloid is seen at 6 hpi. The hypothetical sequence of morphogenesis of the MVA is shown in panels C to I at higher magnifications. (C) Characteristic IV with DNA spot; (D) transition IV→IMV virus; (E) viral form occasionally seen wrapped by two membrane units (arrowhead). In this sequence the traditional stages of maturation of VV are also shown: IMV (F), IEV (G), and EEV (H). (I) Finally, the “transition viral form” IV→IMV is frequently seen out of the cell. Bars: 0.5  $\mu\text{m}$ , A and B; 100 nm, C to I.

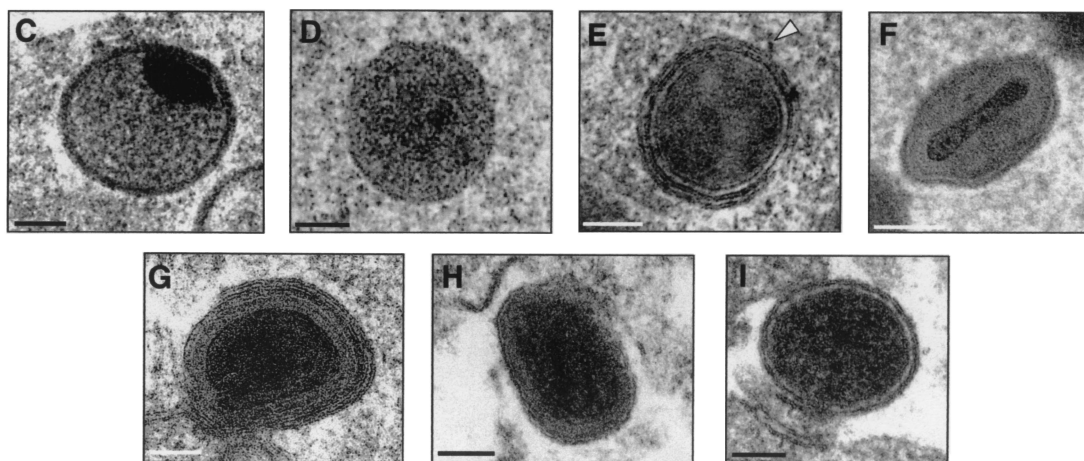


FIG. 7—Continued.

the cell. It has been reported that the WR strain induces cell migration, which is dependent on early genes, and the formation of cellular projections, which requires virus late gene expression (48, 49). The bipolar phenotype that we observed with MVA is not seen in HeLa cells infected with the strains WR, Ankara, and NYCBH (Fig. 4), indicating that MVA viral/or host genes are responsible for the change in cell phenotype. In fact, by microarray analyses of 15,000 human genes, we found a distinct pattern of host gene expression in HeLa cells infected with MVA compared to cells infected with WR strain. The WR strain causes a severe repression of cytoskeleton genes (17); however, infection with MVA induces expression of several cytoskeleton genes that could contribute to the polarized phenotype (unpublished data).

Microbial infections sometimes induce a functional polarization of particular cells via activation of a variety of signaling pathways, depending on the type of microbe (13). However, as shown here, when MVA infects a cell monolayer it induces a dramatic change in cell shape and a major reorganization of the cytoskeleton, changes that could produce a polarized release of virions. This process does not have many precedents in the literature, but something similar could be operating in cells infected with human immunodeficiency virus (HIV). When HIV-infected T lymphocytes are added to epithelial cells, they adhere to, polarize, and secrete virions unidirectionally onto the epithelium (34). The authors of that study speculate that this cytoskeleton-mediated process may participate in HIV transmission *in vivo*. Thus, these two nonrelated viruses are able to trigger signals that transform the structure and function of cytoskeletal elements, which could be used for a polarized release of virions, and minimize exposure to the extracellular medium.

As determined by electron microscopy, MVA assembly in HeLa cells was blocked at the immature virus (IV) stage as described by others (7, 8, 46, 53), but we provide new information that during infection MVA is able to produce further intermediates of virus maturation, with accumulation of non-assembled cytoplasmic viral proteins. It is important to note that our improved preservation techniques for electron microscopy (37–40), together with the examination of intermediates

of virus replication, has made it possible to visualize viral forms not previously described in MVA-infected human HeLa cells.

The study of morphogenetic events in cells infected with the most extensively studied strains of VV—the WR strain and the MVA strain—at early and late times postinfection provided new information on the viral forms produced in HeLa cells, which could be extrapolated when MVA is used as a vaccine in humans. The first stage in the assembly process of MVA is most probably the viral crescent with vesicular elements associated (Fig. 6C), which has been observed previously in cells infected with strain WR (51). This step is followed by a transition stage, found both in cells infected with WR (Fig. 6E) and MVA and in permissive CEFs (Fig. 7D) and nonpermissive HeLa cells (Fig. 8E), and may be a stage that occurs prior to the IMV formation. The transition stage that consists of a dense particle is able to be wrapped by a second envelope (Fig. 6F, 7E, and 8E), which suggests that the protein signals for this phenomenon must be incorporated into these particles and not only in the IMV, as proposed elsewhere (26). In addition, these particles can be found outside of the cells (Fig. 7I), which suggests that they exit the host cell membrane. Similar electron-dense particles were described by Carroll and Moss (7). It is possible that the transition forms can acquire an additional envelope that gives them the capacity to egress from the cell.

A novel potential intermediate form seen in MVA-infected cells is a particle with an assembling core. This intermediate form, which we refer to as “atypical” is rarely seen in cells infected with WR (Fig. 6G) but is most frequently observed in MVA-infected cells (Fig. 7C and F). This atypical virus form, occurring where a complete sealing between the core and the envelope is absent, is very similar to that observed after IMVs from strain WR were treated with the reducing agent dithiothreitol (27). The authors of that study found that membranes around the isolated particles appeared to be less stable and detached from the underlying core. Therefore, it is possible that the intermediate virus form in MVA-infected cells is the same form as that described for WR and that its formation is compatible with reduced interaction between membranes of the envelope with the core structure, where disulfide bonds or other types of protein interaction play roles in maintaining the

## MVA VV/HeLa

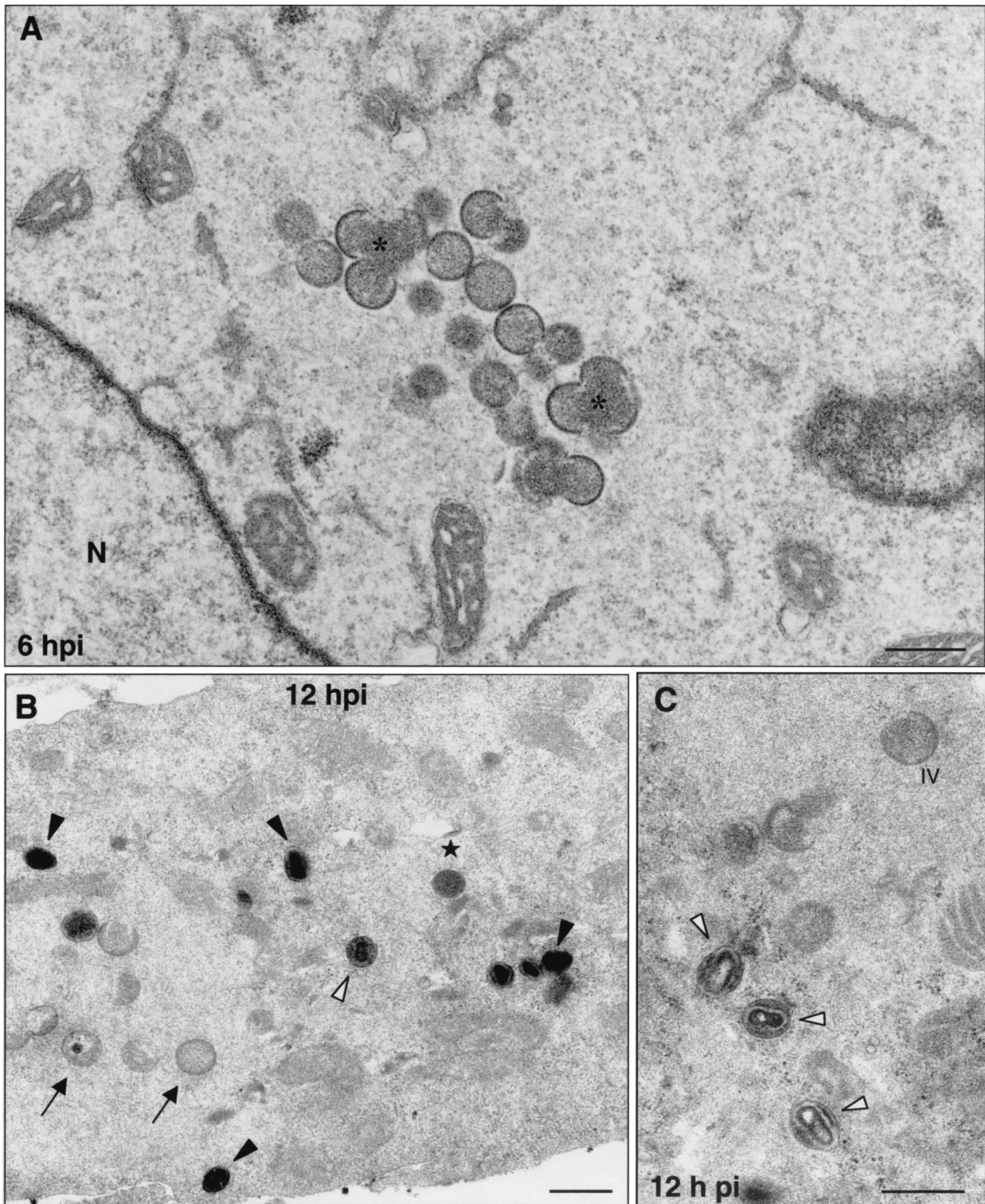


FIG. 8. Morphogenetic events in human cells infected with MVA. HeLa cells were infected (5 PFU/cell) with MVA and processed by electron microscopy as described above. (A) Cell cultures in low-magnification fields show small viroplasm foci and forming IVs (asterisks) at 6 hpi. (B) At 12 hpi, IVs (arrows), transition forms (star), and IMVs (arrowheads) were detected in infected cells. Many of these “IMVs” exhibit an altered internal structure (white arrowheads). The hypothetical sequence of morphogenesis of MVA is shown in panels D to H at higher magnifications. Together with the characteristic IV (D), the spherical and dense transition forms are frequent (E), some of them in the process of being wrapped by additional membranes (arrowhead). (F) Potential transition form occurring prior to the IMV. Note that the IMV (G) is able to initiate the process of wrapping in association with a cisternal compartment (arrowhead in H). Bars: 0.5  $\mu$ m, A and C; 100 nm, D to H; 300 nm.

## MVA VV/HeLa

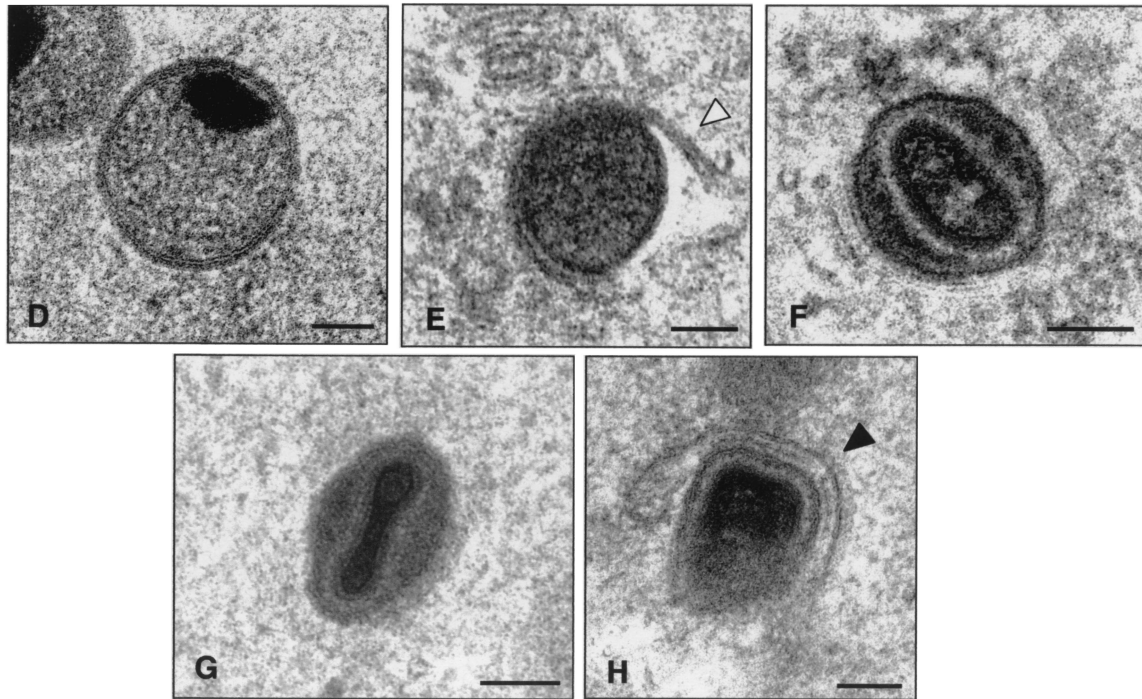


FIG. 8—Continued.

atypical virus form. There appears to be formation, subsequent to the appearance of this viral form, of infectious IMV particles. Indeed, some mature IMV forms were observed in HeLa cells infected with MVA (Fig. 8B and G) but were reduced in amount compared to permissive cells (Fig. 1, 6B, and 7B). These IMVs have a more rounded shape than those derived from HeLa cells infected with the WR or Ankara strains (compare Fig. 6B and 9A with Fig. 7B). The IMVs from MVA-infected HeLa cells are able to initiate the process of wrapping in association to a cisternal compartment to produce an IEV form (Fig. 8H). Formation of some mature infectious virions in HeLa cells infected with MVA is compatible with the virus growth curves (not shown). Although other groups have obtained similar MVA virus growth curves in HeLa cells (4, 7), these groups have not observed some of the viral intermediates that we have described here.

The intermediates that we have observed in HeLa cells infected with WR and MVA were similar in cells infected with the parental wild-type Ankara and with the vaccine strain NYCBH, although differences in the frequency of these intermediates were observed between the VV strains a 12 hpi (Fig. 1). The WR and Ankara strains produced similar intermediates with small variations in the amounts of the different viral forms. MVA and Ankara strains yielded similar percentages of IVs and clear differences in the amounts of IMVs and atypical viral forms (Fig. 1). The vaccine strain NYCBH produced viral intermediates similar to those produced by MVA, but the percentage of atypical virus was reduced in cells infected with NYCBH compared to cells infected with MVA (Fig. 1).

A comparison of the sizes and shapes of purified virions (IMVs) obtained from permissive cells (BHK-21) revealed that

MVA virions are more rounded than those of the other VV strains (Fig. 10). Whereas virions from WR and Ankara had similar sizes and most of them had the typical brick-shaped appearance, virions from NYCBH are frequently found as narrow-brick-shaped particles (Fig. 9 and 10). The differences in size and shape of MVA virions compared to the wild-type Ankara strain could be related to the deletions and/or mutations in the MVA genome.

Considering the data presented here, it is clear that some maturation of MVA is indeed actually taking place in HeLa cells giving rise to atypical forms, IMVs, and IEVs. Some of these mature viruses could be used to infect surrounding cells. Since we have not observed the characteristic actin tails in MVA-infected HeLa cells (Fig. 3 and 4) or in BSC-40 cells (data not shown), how should we explain the infection of neighboring cells as observed in Fig. 5B. It has been described that actin polymerization apparently occurs when the outer membrane of IEV fuses with the plasma membrane and is triggered by the A36R gene product. The actin tails propel the CEV to the adjacent cell for cell-to-cell spread (50). Thus, some cell-to-cell spread in HeLa cells infected with MVA may still be due to a limited production of the IEV form, its fusion with the cell plasma membrane, formation of CEV, and projection via actin tails into neighboring cells. In the absence of characteristic actin tails in MVA-infected HeLa cells, it is possible that the virus uses alternative mechanisms of virus spreading. Indeed, cell-cell fusion through the connecting bridges could provide a mechanism of transport of infectious MVA progeny.

In conclusion, this investigation provides new information on the biology of MVA in nonpermissive human HeLa cells,

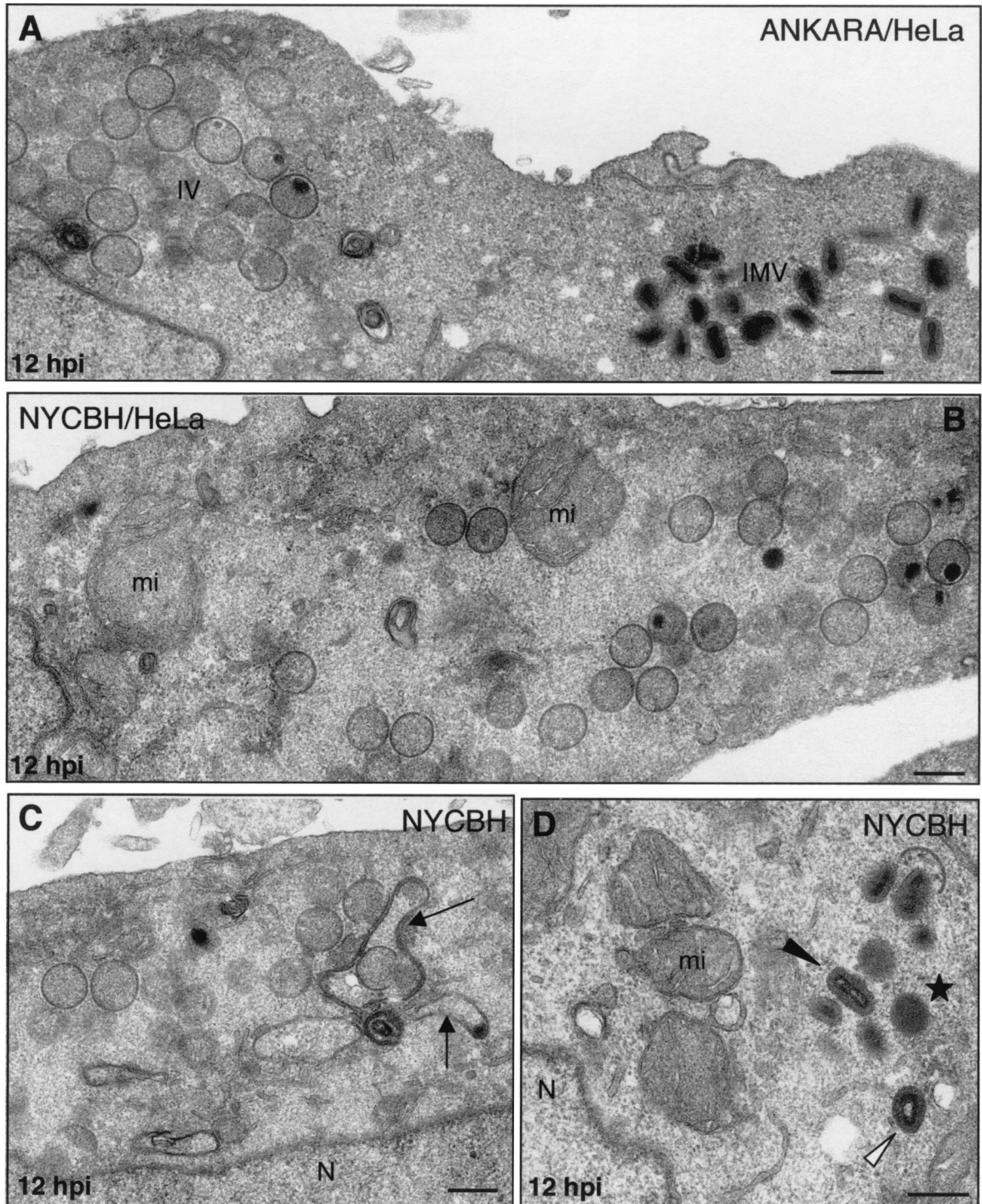


FIG. 9. Assembly of Ankara and NYCBH strains of VV in HeLa cells. HeLa cells were infected with 5 PFU of Ankara or NYCBH strains of VV/cell, and at 12 hpi the cells were processed for electron microscopy analysis. (A) Both IVs and IMVs accumulated in the cytoplasm of HeLa cells infected with Ankara strain. (B) The NYCBH strain accumulated large amounts of IVs in the perinuclear areas of HeLa cells, where numerous swollen mitochondria (mi) are seen. (C and D) In these cells IVs are frequently surrounded by dense membranes (marked by arrows in panel C), and small groups of IMVs (black arrowhead in panel D) close to dense "transition" viral particles (star, panel D) and "atypical IMVs" (white arrowhead in panel D) are frequently seen. N, nucleus. Bars, 300 nm.

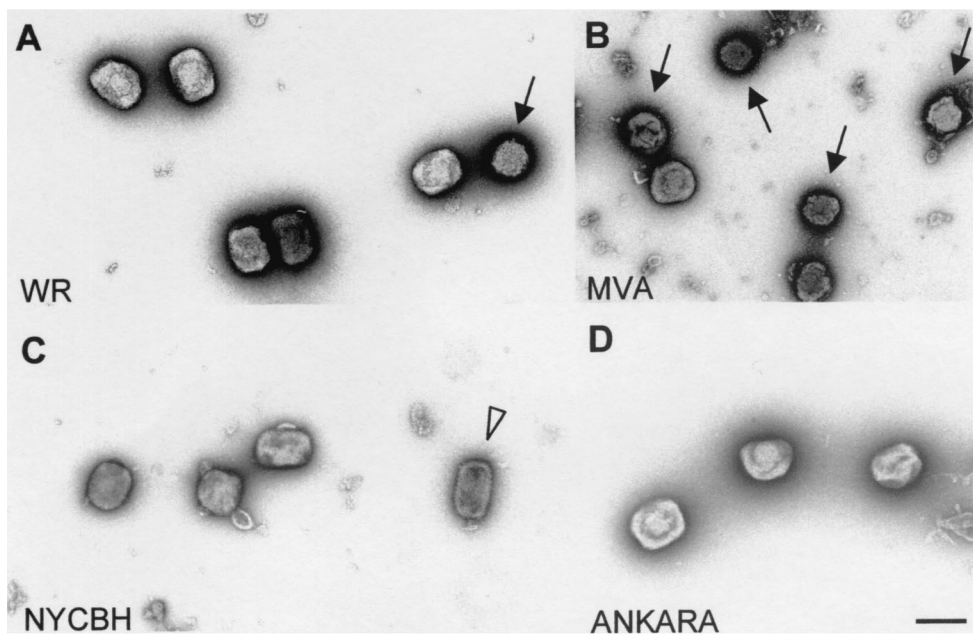


FIG. 10. Morphology and sizes of purified virions from different VV strains (WR [A], MVA [B], Ankara [C], and NYCBH [D]). Sucrose-purified virions isolated from infected BHK-21 cells were negatively stained and processed for electron microscopy. Although the predominant forms for the WR and Ankara strains were brick-shaped particles, rounded forms were occasionally detected for WR (arrow in panel A), being very abundant for MVA (arrows in panel B). The NYCBH and Ankara strains also contain a small percentage of rounded particles and, in the case of NYCBH, a third morphology was seen corresponding to narrow-brick-shaped particles (white arrowhead in panel C). Bar, 300 nm.

demonstrating that MVA induces polarization of infected cells and produces a variety of viral forms. We have also demonstrated differences in the amounts and ultrastructure of the viral forms with respect to those found in HeLa cells infected with the different VV strains, including the WR, Ankara, and NYCBH strains.

#### ACKNOWLEDGMENTS

This study was supported by the following grants: BIO99-0803 (D.R.) and BIO2001-2269 from the Ministerio de Ciencia y Tecnología, FIPSE 36344/02 Spain from EuroVac, QLRT-PL-1999-01321 and QLK2-CT2002-01867 from the European Union (M.E.), and 08.2/0042.2/2000 from the Comunidad Autónoma de Madrid (C.R. and D.R.). J.C.G.-G. was supported by a predoctoral fellowship.

We thank María Angeles Muñoz and Carlos Sánchez (Confocal Service of Centro de Biología Molecular "Severo Ochoa") and Silvia Gutierrez (Confocal Service of Centro Nacional de Biotecnología) for help in capturing images and Victoria Jiménez for expert technical assistance with tissue culture cells and virus growth.

#### REFERENCES

- Alcami, A., A. Khanna, N. L. Paul, and G. L. Smith. 1999. Vaccinia virus strains Lister, USSR and Evans express soluble and cell-surface tumour necrosis factor receptors. *J. Gen. Virol.* **80**:949–959.
- Amara, R. R., J. M. Smith, S. I. Staprans, D. C. Montefiori, F. Villinger, J. D. Altman, S. P. O'Neil, N. L. Kozyr, Y. Xu, L. S. Wyatt, P. L. Earl, J. G. Herndon, J. M. McNicholl, H. M. McClure, B. Moss, and H. L. Robinson. 2002. Critical role for Env as well as Gag-Pol in control of a simian-human immunodeficiency virus 89.6P challenge by a DNA prime/recombinant modified vaccinia virus Ankara vaccine. *J. Virol.* **76**:6138–6146.
- Antoine, G., F. Scheiffinger, F. Dörner, and F. G. Falkner. 1998. The complete genomic sequence of the modified vaccinia Ankara strain: comparison with other orthopoxviruses. *Virology* **244**:365–396.
- Blanchard, T. J., A. Alcami, P. Andrea, and G. L. Smith. 1998. Modified vaccinia virus Ankara undergoes limited replication in human cells and lacks several immunomodulatory proteins: implications for use as a human vaccine. *J. Gen. Virol.* **79**:1159–1167.
- Belsham, G. J., J. K. Brangwyn, M. D. Ryan, C. C. Abrams, and A. M. King. 1990. Intracellular expression and processing of foot-and-mouth disease virus capsid precursors using vaccinia virus vectors: influence of the L protease. *Virology* **176**:524–530.
- Broder, C. C., and P. L. Earl. 1997. Design and construction of recombinant vaccinia viruses. *Methods Mol. Biol.* **62**:173–197.
- Carroll, M. W., and B. Moss. 1997. Host range and cytopathogenicity of the highly attenuated MVA strain of vaccinia virus: propagation and generation of recombinant viruses in a nonhuman mammalian cell line. *Virology* **238**:198–211.
- Carroll, M. W., W. W. Overwijk, R. S. Chamberlain, S. A. Rosenberg, B. Moss, and N. P. Restifo. 1997. Highly attenuated modified vaccinia virus Ankara (MVA) as an effective recombinant vector: a murine tumor model. *Vaccine* **15**:387–394.
- Cau, J., S. Faure, M. Comps, C. Delsert, and N. Morin. 2001. A novel p21-activated kinase binds the actin and microtubule networks and induces microtubule stabilization. *J. Cell Biol.* **155**:1029–1042.
- Choudhury, S., M. A. el Farrash, M. J. Kuroda, and S. Harada. 1996. Retention of HIV-1 inside infected MOLT-4 cells in association with adhesion-induced cytoskeleton reorganization. *AIDS* **10**:363–368.
- Coupar, B. E., M. E. Andrew, and D. B. Boyle. 1988. A general method for the construction of recombinant vaccinia viruses expressing multiple foreign genes. *Gene* **68**:1–10.
- Dales, S., and L. Siminovitch. 1961. The development of vaccinia virus in Earles L strain cells as examined by electron microscopy. *J. Biophys. Biochem. Cytol.* **10**:475–503.
- de Jong, E. C., P. L. Vieira, P. Kalinski, J. H. Schuitemaker, Y. Tanaka, E. A. Wierenga, M. Yazdanbakhsh, and M. L. Kapsenberg. 2002. Microbial compounds selectively induce Th1 cell-promoting or Th2 cell-promoting dendritic cells in vitro with diverse th cell-polarizing signals. *J. Immunol.* **168**:1704–1709.
- Earl, P. L., N. Cooper, L. S. Wyatt, B. Moss, and M. W. Carroll. 1998. Titration of MVA stocks by immunostaining, p. 16.9–16.11. *In* F. M. Ausubel, R. E. Kingston, D. D. Moore, J. G. Seidman, J. A. Smith, and K. Struhl (ed.), *Current protocols in molecular biology*. Greene/Wiley Interscience, New York, N.Y.
- Esteban, M., and C. Patino. 2000. Identification by electron microscopy of the maturation steps in vaccinia virus morphogenesis inhibited by the interferon-induced enzymes, protein kinase (PKR), 2–5A synthetase, and nitric oxide synthase (iNOS). *J. Interferon Cytokine Res.* **20**:867–877.
- Flint, S. J., L. W. Enquist, R. M. Krug, V. R. Racaniello, and A. M. Skalka (ed.). 2000. Prevention and control of viral disease, p. 663–714. *In* Principles of virology: molecular biology, pathogenesis, and control. ASM Press, Washington, D.C.



17. Guerra, S., L. A. López-Fernandez, A. Pacual-Montano, M. Muñoz, K. Harshman, and M. Esteban. 2003. Cellular gene expression survey of vaccinia virus infection of human HeLa cells. *J. Virol.* **77**:6493–6506.
18. Gulley, J., A. P. Chen, W. Dahut, P. M. Arlen, A. Bastian, S. M. Steinberg, K. Tsang, D. Panicali, D. Poole, J. Schlom, and H. J. Michael. 2002. Phase I study of a vaccine using recombinant vaccinia virus expressing PSA (rV-PSA) in patients with metastatic androgen-independent prostate cancer. *Prostate* **53**:109–117.
19. Griffiths, G., N. Ross, S. Schleich, and J. Krijnse-Locker. 2001. Structure and assembly of intracellular vaccinia virus: thin-section analysis. *J. Virol.* **75**:11056–11070.
20. Heljasvaara, R., D. Rodriguez, C. Risco, J. L. Carrascosa, M. Esteban, and J. R. Rodriguez. 2001. The major core protein P4a (A10L gene) of vaccinia virus is essential for correct assembly of viral DNA into the nucleoprotein complex to form immature viral particles. *J. Virol.* **75**:5778–5795.
21. Hollinshead, M., G. Rodger, H. van Eijl, M. Law, R. Hollinshead, D. J. Vaux, and G. L. Smith. 2001. Vaccinia virus utilizes microtubules for movement to the cell surface. *J. Cell Biol.* **154**:389–402.
22. Hollinshead, M., A. Vandersplassen, G. L. Smith, and D. J. Vaux. 1999. Vaccinia virus intracellular virions contain only one lipid membrane. *J. Virol.* **73**:1503–1517.
23. Honore, B., P. Madsen, H. H. Rasmussen, J. Vandekerckhove, J. E. Celis, and H. Leffers. 1993. Cloning and expression of a cDNA covering the complete coding region of the P32 subunit of human pre-mRNA splicing factor SF2. *Gene* **134**:283–287.
24. Houhou, L., A. Lamouroux, N. F. Biguet, and J. Mallet. 1995. Expression of human dopamine beta-hydroxylase in mammalian cells infected by recombinant vaccinia virus: mechanisms for membrane attachment. *J. Biol. Chem.* **270**:12601–12606.
25. Joklik, W., and Y. Becker. 1964. The replication and coating of vaccinia DNA. *J. Mol. Biol.* **10**:452–474.
26. Krijnse-Locker, J., A. Kuehn, S. Schleich, G. Rutter, H. Hohenberg, R. Wepf, and G. Griffiths. 2000. Entry of the two infectious forms of vaccinia virus at the plasma membrane is signaling-dependent for the IMV but not the EEV. *Mol. Biol. Cell* **11**:2497–2511.
27. Krijnse-Locker, J., and G. Griffiths. 1999. An unconventional role for the cytoplasmic disulfide bonds in vaccinia virus proteins. *J. Cell Biol.* **144**:267–279.
28. Mallardo, M., S. Schleich, and L. J. Krijnse. 2001. Microtubule-dependent organization of vaccinia virus core-derived early mRNAs into distinct cytoplasmic structures. *Mol. Biol. Cell* **12**:3875–3891.
29. Moreau, V., F. Frischknecht, I. Reckmann, R. Vincentelli, G. Rabut, D. Stewart, and M. Way. 2000. A complex of N-WASP and WIP integrates signalling cascades that lead to actin polymerization. *Nat. Cell Biol.* **2**:441–448.
30. Morgan, C. 1976. Vaccinia virus reexamined: development and release. *Virology* **73**:43–58.
31. Moss, B. 2001. *Poxviridae*: the viruses and their replication, p. 1249–1283. In D. M. Knipe and P. M. Howley (ed.), *Fields virology*. Lippincott/The Williams & Wilkins Co., Philadelphia, Pa.
32. Moss, B., and B. M. Ward. 2001. High-speed mass transit for poxviruses on microtubules. *Nat. Cell Biol.* **3**:E245–E246.
33. Nilsson, C., G. Sutter, L. Walther-Jallow, P. ten Haaf, L. Akerblom, J. Heeney, V. Erfle, P. Bottiger, G. Biberfeld, and R. Thorstensson. 2002. Immunization with recombinant modified vaccinia virus Ankara can modify mucosal simian immunodeficiency virus infection and delay disease progression in macaques. *J. Gen. Virol.* **83**:807–818.
34. Pearce-Pratt, R., D. Malamud, and D. M. Phillips. 1994. Role of the cytoskeleton in cell-to-cell transmission of human immunodeficiency virus. *J. Virol.* **68**:2898–2905.
35. Perkus, M. E., A. Piccini, B. R. Lipinskas, and E. Paoletti. 1985. Recombinant vaccinia virus: immunization against multiple pathogen. *Science* **229**:981–984.
36. Ramirez, J. C., M. M. Gherardi, and M. Esteban. 2000. Biology of attenuated modified vaccinia virus Ankara recombinant vector in mice: virus fate and activation of B- and T-cell immune responses in comparison with the Western Reserve strain and advantages as a vaccine. *J. Virol.* **74**:923–933.
37. Risco, C., J. R. Rodriguez, C. Lopez-Iglesias, J. L. Carrascosa, M. Esteban, and D. Rodriguez. 2002. Endoplasmic reticulum-Golgi intermediate compartment membranes and vimentin filaments participate in vaccinia virus assembly. *J. Virol.* **76**:1839–1855.
38. Risco, C., and J. L. Carrascosa. 1999. Visualization of viral assembly in the infected cell. *Histol. Histopathol.* **14**:905–926.
39. Risco, C., J. R. Rodriguez, W. Demkowicz, R. Heljasvaara, J. L. Carrascosa, M. Esteban, and D. Rodriguez. 1999. The vaccinia virus 39-kDa protein forms a stable complex with the p4a/4a major core protein early in morphogenesis. *Virology* **265**:375–386.
40. Risco, C., M. Muntión, L. Enjuanes, and J. L. Carrascosa. 1998. Two types of virus-related particles are found during transmissible gastroenteritis virus morphogenesis. *J. Virol.* **72**:4022–4031.
41. Rodger, G., and G. L. Smith. 2002. Replacing the SCR domains of vaccinia virus protein B5R with EGFP causes a reduction in plaque size and actin tail formation but enveloped virions are still transported to the cell surface. *J. Gen. Virol.* **83**:323–332.
42. Rodriguez, J. F., and G. L. Smith. 1990. Inducible gene expression from vaccinia virus vectors. *Virology* **177**:239–250.
43. Rodriguez, J. R., C. Risco, J. L. Carrascosa, M. Esteban, and D. Rodriguez. 1998. Vaccinia virus 15-kilodalton (A14L) protein is essential for assembly and attachment of viral crescents to virosomes. *J. Virol.* **72**:1287–1296.
44. Rodriguez, D., C. Risco, J. R. Rodriguez, J. L. Carrascosa, and M. Esteban. 1996. Inducible expression of the vaccinia virus A17L gene provides a synchronized system to monitor sorting of viral proteins during morphogenesis. *J. Virol.* **70**:7641–7653.
45. Rodriguez, D., M. Esteban, and J. R. Rodriguez. 1995. Vaccinia virus A17L gene product is essential for an early step in virion morphogenesis. *J. Virol.* **69**:4640–4648.
46. Sancho, M. C., S. Schleich, G. Griffiths, and J. Krijnse-Locker. 2002. The block in assembly of modified vaccinia virus Ankara in HeLa cells reveals new insights into vaccinia virus morphogenesis. *J. Virol.* **76**:8318–8334.
47. Sanderson, C. M., M. Hollinshead, and G. L. Smith. 2000. The vaccinia virus A27L protein is needed for the microtubule-dependent transport of intracellular mature virus particles. *J. Gen. Virol.* **81**:47–58.
48. Sanderson, C., M. Way, and G. L. Smith. 1998. Virus-induced cell motility. *J. Virol.* **72**:1235–1243.
49. Sanderson, C., and G. L. Smith. 1998. Vaccinia virus induces Ca<sup>2+</sup>-independent cell-matrix adhesion during the motile phase of infection. *J. Virol.* **72**:9924–9933.
50. Smith, G. L., A. Vandersplassen, and M. Law. 2002. The formation and function of extracellular enveloped vaccinia virus. *J. Gen. Virol.* **83**:2915–2931.
51. Sodeik, B., R. W. Doms, M. Ericsson, G. Hiller, C. E. Machamer, W. van't Hof, G. van Meer, B. Moss, and G. Griffiths. 1993. Assembly of vaccinia virus: role of the intermediate compartment between the endoplasmic reticulum and the Golgi stacks. *J. Cell Biol.* **121**:521–541.
52. Sodeik, B., and J. Krijnse-Locker. 2002. Assembly of vaccinia virus revisited: de novo membrane synthesis or acquisition from the host? *Trends Microbiol.* **10**:15–24.
53. Sutter, G., and B. Moss. 1992. Nonreplicating vaccinia vector efficiently expresses recombinant genes. *Proc. Natl. Acad. Sci. USA* **89**:10847–10851.
54. Tolonen, N., L. Doglio, S. Schleich, and L. J. Krijnse. 2001. Vaccinia virus DNA replication occurs in endoplasmic reticulum-enclosed cytoplasmic mini-nuclei. *Mol. Biol. Cell* **12**:2031–2046.